学　位　論　文

Development of a novel cancer therapy with a ferroptosis inducer and radiation, and a prediction method for therapeutic effects targeting ferroptosis

（フェロトーシス誘導剤と放射線を併用した新規がん治療法、及びフェロトーシス誘導がん治療効果予測法の開発）

2020 年 3 月

北　海　道　大　学

柴田　悠貴

Yuki Shibata

学　位　論　文

Development of a novel cancer therapy with a ferroptosis inducer and radiation, and a prediction method for therapeutic effects targeting ferroptosis

（フェロトーシス誘導剤と放射線照射を併用した新規がん治療法、及びフェロトーシス誘導がん治療効果予測法の開発）

2020 年 3 月

北　海　道　大　学

柴田　悠貴

Yuki Shibata

Table of Contents

List of Publications and Presentations

Part of this research was published in the following paper.

1. Shibata, Y., Yasui, H., Higashikawa, K., Miyamoto, N., Kuge, Y. Erastin, a ferroptosis-inducing agent, sensitized cancer cells to X-ray irradiation via glutathione starvation *in vitro* and *in vivo*. PLoS ONE 14(12): e0225931.

Part of this research was presented at the following conferences.

1. Shibata, Y., Yasui, H., Higashikawa, K., Kuge, Y. A basic study on PET imaging technique for predicting cancer sensitivity to ferroptosis-targeting cancer therapy. Society for Redox Biology and Medicine's 26th Annual Conference, November 2019, Las Vegas, NV.

2. Shibata, Y., Yasui, H., Higashikawa, K., Miyamoto, N., Kuge, Y. Evaluation of erastin, a ferroptosis inducer, as a sensitizer for X-irradiation treatment against human adenocarcinoma. The 7th GI-CoRE Medical Science and Engineering Symposium, August 2019, Sapporo, JAPAN.

3. Shibata, Y., Yasui, H., Higashikawa, K., Miyamoto, N., Kuge, Y. Evaluation of ferroptosis-targeting cancer therapy in combination with radiation. The 72nd Annual Meeting of Society for Free Radical Research Japan, June 2019, Sapporo, JAPAN.

4. Shibata, Y., Yasui, H., Higashikawa, K., Kuge, Y. Basic study on developing a prediction method for ferroptosis-targeting therapy against cancer. 14th Annual Meeting of the Japanese Society for Molecular Imaging, May 2019, Sapporo, JAPAN.

5. Shibata, Y., Yasui, H., Higashikawa, K., Kuge, Y. Investigation of radiosensitizing effect by erastin, a ferroptosis inducer in cancer cells. 138th Annual Meeting of the Pharmaceutical Society of Japan, March 2018, Ishikawa, JAPAN.

List of Abbreviations

aTf: apo transferrin

BSO: buthionine sulfoximine

DMSO: dimethyl sulfoxide

D_{10}: 10% lethal dose

EDTA: ethylenediaminetetraacetic acid

GSH: reduced form glutathione

GSSG: oxidized form glutathione

GPX4: glutathione peroxidase 4

HEPES: 2-[4-(2-hydroxyethyl)piperazin-1-yl] ethanesulfonic acid

HPLC: high-performance liquid chromatography

hTf: holo transferrin

ICP-AES: inductively coupled plasma atomic emission spectrometry

LQ: linear quadratic

MALDI-TOF-MS: Matrix-assisted laser desorption-ionization time-of-flight mass spectrometry

NOTA: p-isothiocyanatobenzyl-1,4,7-triazacyclononane-1,4,7-triacetic acid

PBS: phosphate buffered-saline

PET: positron emission tomography

ROS: reactive oxygen species

SDS-PAGE: sodium dodecyl sulfate polyacryl amide gel electrophoresis

Tf: transferrin

TLC: thin-layer chromatography

TfR1: transferrin receptor 1

xCT: cystine/glutamate antiporter

Preface

Cancer therapy resistance has become a serious issue in clinical practice. One conceivable cause of the therapy resistance is that cancers with genomic instability can easily acquire resistance to drugs through adaptive response and reduce their therapeutic effect (Swanton, 2012; Holohan et al., 2013). To overcome this problem, development of a novel anticancer strategy to induce cancer cell death through a mechanism different from conventional drugs is thought to be an urgent and required challenge. Recently, a novel programmed cell death triggered by iron-dependent accumulation of lipid hydroperoxide, called as ferroptosis, has been discovered and gaining attention as a novel cancer therapeutic target (Dixon et al., 2012). Ferroptosis is distinct from other well-known forms of cell death, such as apoptosis, necrosis, and autophagy, owing to its iron dependence. Iron is an essential nutrient for mammalian organism. In addition to the function of iron to bind hemoglobin and carry oxygen throughout the body, it functions as the active center of various biological enzymes such as cytochrome p450 which is required for drug metabolism and ribonucleotide reductase which is involved in DNA synthesis. In cancer cells, iron homeostasis is often disrupted, which leads to excessive iron accumulation (Bystrom et al., 2015), partially because that iron is essential for maintaining the aberrantly high growth rate of cancer cells by supplying the iron-

dependent enzyme ribonucleotide reductase (Elford et al., 1970). Besides, iron-dependent ferroptosis can be induced by inhibiting cystine/glutamate antiporter (xCT) or glutathione peroxidase 4 (GPX4), which plays an important role in the cellular antioxidant network (Yang et al., 2014; Xie et al., 2016) (Fig 1). Erastin, an inducer of ferroptosis discovered at first, has an antitumor effect through xCT inhibition (Yang et al., 2008). Moreover, some tumors have shown a strong dependence on xCT and GPX4 for ferroptosis induction in the past studies (Conrad et al., 2016; Lu et al., 2018). As the cell death is strictly regulated by iron accumulation and antioxidant productive capability as described above, induction of ferroptosis will be a useful approach to the cancer therapy.

In this study, I aimed to establish a precision medicine system for a novel effective cancer therapeutic strategy targeting ferroptosis. For achieving this objective, in Chapter 1, I investigated cancer therapeutic effect of ferroptosis inducer erastin combined with radiation. Previous studies have reported that the combination of ferroptosis inducers with other anticancer drugs enhanced the therapeutic effects on chemotherapy-resistant cancers (Roh et al., 2016; Yu et al., 2015; Chen et al., 2015). I hypothesized that erastin may also enhance the effects of cancer radiotherapy by the similar mechanism of chemosensitizing effect. Therefore, I evaluated the radiosensitizing effect of erastin on human adenocarcinoma cell lines. From this study, I revealed that combination treatment

of erastin and X-irradiation efficiently suppresses the tumor growth by glutathione depletion. Thus, my study suggested that the ferroptosis-targeting cancer therapy exerts a significant therapeutic effect combined with radiotherapy. Although, due to the diversity of characteristics of cancers, the sensitivity to ferroptosis inducers is expected to be different (Yang et al., 2014; Lu et al., 2017). Therefore, therapeutic effects of ferroptosis inducers are expected to vary among patients. However, there is still no method for diagnosing them. To apply the ferroptosis-targeting cancer therapy effectively to individual patients, an indicator for selecting this therapeutic strategy from a number of molecular targeting drugs is needed. Thus, in chapter 2, I conducted a basic study on developing a diagnostic technique of nuclear medicine for predicting effect of ferroptosis-targeting cancer therapy. Transferrin receptor 1 (TfR1) is a key molecule for cellular iron homeostasis and ferroptosis. By focusing on TfR1 as a target for the diagnosis, I succeeded to indicate the potentials of transferrin-based nuclear imaging probe to predict cancer sensitivity of erastin for the first time in the world. From these studies, usefulness of a novel effective cancer therapeutic strategy by targeting ferroptosis induction and a novel diagnostic method for predicting anticancer effect of ferroptosis inducer has been suggested, which may contribute as a first step toward the development of precision medicine system.

The results in chapter 1 of this doctoral thesis has already been published in PLoS ONE journal (Shibata et al., 2019), and the chapter 2 are currently being prepared for submission to an international journal.

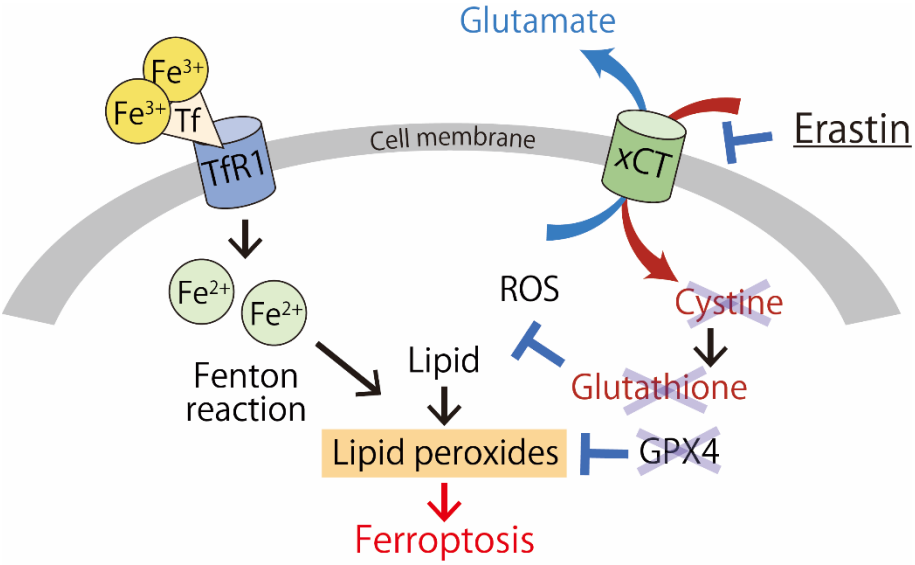

Fig 1. Outline of eratin's cytotoxic mechanism.

Abbreviations: GPX4 = Glutathione peroxidase 4; ROS = Reactive oxygen species; TfR1 = Transferrin receptor 1; xCT = cystine/glutamate antiporter. Ferroptosis is triggered by iron dependent accumulation of lipid peroxides. Erastin treatment inhibits cellular glutathione synthesis and GPX4 activation by a loss of cystine uptake.

Chapter 1

Investigation of ferroptosis-targeting cancer therapy combined with X-ray irradiation

Introduction

As mentioned above, cancer cells have abundant amount of iron and are therefore often exposed to excessive oxidative stress. However, cancer cells produce sufficient amounts of antioxidants, such as glutathione, to protect themselves from oxidative stress (Traverso et al., 2013). Therefore, high concentrations of antioxidants are a major obstacle to cancer chemotherapy and radiotherapy (Bansal and Simon, 2018). To overcome this therapy resistance, strategies targeting antioxidant depletion have been widely investigated. For example, buthionine sulfoximine (BSO), a well known synthetic glutathione inhibitor, was reported to show a chemosensitizing effect in myeloma and neck cancers (Tagde et al., 2014). Moreover, a combination of BSO and melphalan, a nitrogen mustard alkylating agent, is used on neuroblastoma patients in clinical trials (Villablanca et al., 2016).

As cell death is strictly regulated by iron accumulation and antioxidant production capability of cancer cells, which are abundant in iron, induction of iron-dependent form of cell death, ferroptosis, is a useful approach to cancer therapy. Erastin,

an inducer of ferroptosis, is identified as an inhibitor of xCT and glutathione synthesis (Dixon et al., 2014). In addition, sulfasalazine, a clinical drug for inflammatory bowel disease, is an xCT inhibitor that induces ferroptosis (Dixon et al., 2012). These drugs have an antitumor effect by ferroptosis induction (Lu et al., 2017; Sontheimer and Bridges, 2012; Mooney et al., 2019). In addition, these ferroptosis inducers can enhance the effect of chemotherapeutic agents such as cisplatin and temozolomide (Roh et al., 2016; Yu et al., 2015; Chen et al., 2015). However, there are only a few studies on the efficacy of the treatment with a combination of these ferroptosis inducers and X-ray irradiation. In this study, I hypothesized that erastin modulates a ferroptosis-related pathway and affects the sensitivity of cancer cells to X-ray irradiation-induced cell death. The hypothesis was tested *in vitro* and *in vivo* using two human cancer cell lines.

Materials and methods

Reagents

Erastin was purchased from AdooQ Bioscience (Irvine, CA) and ferrostatin-1 from Sigma-Aldrich (St. Louis, MO). The following antibodies were used for western blotting: anti-glutathione peroxidase 4 (Cat. No. ab125066, Abcam, Cambridge, UK), anti-β-actin (Sigma-Aldrich), and horseradish peroxidase-conjugated secondary

antibodies (Promega, Madison, WI).

Cell culture

Human cervical adenocarcinoma cells (HeLa) and lung adenocarcinoma cells (NCI-H1975) were purchased from the RIKEN Cell Bank (Tsukuba, Japan) and American Type Culture Collection (Manassas, VA), respectively. These cells were grown in the RPMI-1640 medium (Sigma-Aldrich) supplemented with 10% fetal bovine serum (CELLect®, MP Biomedicals, Santa Ana, CA) and 100 units/mL of penicillin-streptomycin (MP Biomedicals). The cells were maintained at 37°C in 5% CO_2.

X-ray irradiation and drug treatment

Cells were irradiated with X-rays using a linear accelerator (CLINAC 6EX, Varian Medical Systems, Palo Alto, CA) at doses of 2.5, 5.0, 7.5, and 10 Gy (dose rate, 2.19 Gy/min). The prescribed dose was defined at the isocenter. HeLa and NCI-H1975 cells in plastic dishes (60 or 90 mm i.d.) were allowed to adhere to the dishes at 37°C in 5% CO_2 for 6 h. Subsequently, they were treated with erastin alone (0.1, 1, 5, 10, 20, or 50 μM) or with erastin and ferrostatin-1 (1 μM) and incubated for 24 h.

Clonogenic survival assay

An appropriate number of tumor cells attached to 60 mm dishes were treated with erastin alone or combination with ferrostatin-1 and/or X-ray irradiation. After the treatment, the compounds were removed by replacing the medium with a fresh one and the cells were incubated in a humidified 5% CO_2 atmosphere at 37°C for nine days. The cell colonies were fixed with methanol, stained with the Giemsa solution, and counted under a microscope (CKX41, Olympus, Tokyo, Japan). Only the colonies containing more than 50 cells were counted as surviving colonies. The survival curves were fit to a linear-quadratic (LQ) model using the data analysis software GraphPad Prism 7 (GraphPad Software Inc., San Diego, CA).

Sodium dodecyl sulfate polyacryl amide gel electrophoresis (SDS-PAGE) and western blotting

The HeLa and NCI-H1975 cells were collected and lysed in a RIPA buffer (Thermo Fisher Scientific, Carlsbad, CA) with a protease inhibitor cocktail (Roche Diagnostics, Basel, Switzerland) and subjected to two freeze–thaw cycles. The lysed cells were centrifuged at 15,000×*g* for 20 min at 4°C, and the supernatants were collected as protein samples. Laemmli's sample buffer (Bio-Rad, Hercules, CA) was added to the

supernatants, and the mixture was boiled for 5 min. Proteins were separated by SDS-PAGE and transferred onto a PVDF membrane (Bio-Rad) at 60 V in a transfer buffer (25 mM Tris, 192 mM glycine, and 20% methanol) for 60 min at 4°C. The membrane was probed overnight with specific antibodies (anti-glutathione peroxidase 4 or anti-β-actin) diluted with TBST (10 mM Tris-HCl [pH 7.4], 0.1 M NaCl and 0.1% Tween-20) containing 5% skim milk (Wako Pure Chemical Industries, Osaka, Japan) at 4°C. After probing with HRP-conjugated secondary antibodies, the bound antibodies were detected with an Immobilon® western HRP substrate (MilliporeSigma, Burlington, MA). Densitometry was performed using Multi Gauge V3.0 software (Fujifilm, Tokyo, Japan).

Measurement of glutathione concentration

Concentrations of the reduced (GSH) and oxidized (GSSG) forms of glutathione were determined with a GSSG/GSH quantification kit (Dojindo Laboratories, Kumamoto, Japan). The harvested cells were lysed in 10 mM HCl and 1% 5-sulfosalicylic acid dihydrate (Wako Pure Chemical Industries). The lysate was centrifuged (8,000×*g*) and the supernatant was collected. An equal volume of H_2O was added to the supernatant and the mixture was incubated with coloring agents. The tumor tissues were lysed in 5% 5-sulfosalicylic acid dihydrate and homogenized with a beads cell disrupter MS-100R

(Tomy Seiko Co., Ltd., Tokyo, Japan). After the lysate was centrifuged, the supernatant was collected and added H_2O up to a final concentration of 0.5% 5-sulfosalicylic acid. The supernatant with 0.5% 5-sulfosalicylic acid was incubated with coloring agents as described above. The absorption of DTNB (λ_{max} = 412 nm) was measured with a multi mode plate reader PowerScan HT (DS Pharma Biomedical Co., Ltd., Osaka, Japan), and concentrations of GSH and GSSG were estimated in accordance with the manufacturer's protocol.

Tumor transplantation

All animal experiments were performed in accordance with the Guideline for Animal Experiments of Hokkaido University, and approved by the Laboratory Animal Care and Use Committee of Hokkaido University (Approval number 16-0102, 18-0111). The mice were housed in a 12-h light/12-h dark cycle with food and water supplied ad libitum. Female BALB/c Slc-nu/nu mice aged 8–10 weeks were purchased from Japan SLC (Hamamatsu, Japan). The NCI-H1975 cells (5×10^6 cells/100 μL of Phosphate-Buffered Saline [PBS]) were inoculated subcutaneously into the left forelimbs of the mice under anesthesia induced with 2% isoflurane. The tumor size was measured using a caliper every other day from 6 days after cell inoculation and calculated as V (mm^3) = (L

× W^2)/2, where L and W are the tumor length and width, respectively. Tumor-transplanted mice were ethically sacrificed when the tumor volume reached at 2,000 mm^3 or a tumor burden greater than 10% of the body weight. The mice were sacrificed by cervical dislocation under 2% isoflurane anesthesia.

Drug administration and X-ray irradiation of mice

Ten days after the inoculation, when the tumor size reached approximately 100 mm^3, the mice were randomly divided into four groups. In accordance with a previous study (Luo et al., 2018), erastin was dissolved in 5% dimethyl sulfoxide (DMSO)/corn oil and intraperitoneally injected into the NCI-H1975 cell-transplanted mice at a dose of 15 mg/kg/day for 3 days at 24-h intervals. For the combination therapy, 24 h after the last erastin injection, the NCI-H1975 cell-transplanted mice were locally irradiated with X-rays at a dose of 3 Gy (dose rate, 4.79 Gy/min) under 1.5% isoflurane anesthesia.

Measurement of intracellular iron

The concentration of intracellular iron was determined by multiple inductively coupled plasma atomic emission spectrometry (ICP-AES) (ICPE-9000, Shimadzu, Tokyo, Japan) according to the method reported by Albanese and others (Albanese et al., 2013).

HeLa and NCI-H1975 cells were seeded in 150 mm dishes 16 h before erastin treatment. After 24 h erastin (0 – 10 μM) treatment, cells were trypsinized and the number of cells were counted. Cells were centrifuged at 200×*g*, 3 min at 4°C and washed with PBS for twice. Samples were stored at -80°C deep freezer. On the day of the ICP-AES analysis, cell samples were lysed with 600 μL 60% ultra-high purity nitric acid (KANTO CHEMICAL Co., Inc., Tokyo, Japan) and incubated for 30 min at 70°C. Samples were then chilled with ice for 1 min and diluted with 8,400 μL Milli-Q water (Merk Millipore) before sample injection to ICPE-9000. In order to calculate iron concentration, iron standard solution (AccuStandard Inc., New Haven, CT) was prepared at 5, 10, 50, 100, 500 ppm.

Statistical analysis

All results are expressed as the mean ± S.E. The statistical analysis was performed using GraphPad Prism 7. The statistical significance of erastin cytotoxicity and the inhibitory effect of ferrostatin-1 on the two cell lines were examined with two-way ANOVA (Fig 2). Multiple comparisons were performed with Tukey–Kramer test (Fig 3). The statistical significance of the therapeutic effects of erastin and the X-ray irradiation on the cancer cell lines were examined with two-way ANOVA (Fig 4). The

therapeutic effects of erastin, X-ray irradiation, and combination treatment against NCI-H1975 cell-transplanted mice were statistically evaluated with repeated-measures two-way ANOVA (Fig 5A). Differences in intratumoral glutathione concentration between the control and erastin-treated groups were evaluated with Student's t-test (Fig 5B). Multiple comparisons of TfR1 protein expression levels and intracellular iron concentrations were analyzed with Tukey–Kramer test (Fig 6). A p-value < 0.05 was considered significant.

Results

Erastin induces ferroptosis in the human adenocarcinoma cell lines.

The toxicity of erastin and its dependency on ferroptosis in human adenocarcinoma cells derived from different organs (HeLa and NCI-H1975 cells) were examined. Erastin cytotoxicity was dose-dependent in both the HeLa and NCI-H1975 cells, and their 50% growth inhibitory concentrations were approximately 3.5 and 5 μM, respectively (Fig 2). In addition, the erastin-induced cell death was significantly inhibited by 1 μM ferrostatin-1, a specific inhibitor of ferroptosis, in both the cell lines (two-way ANOVA, $p < 0.0001$ for treatment with erastin and $p < 0.0001$ for treatment with

ferrostatin-1, in both the HeLa and NCI-H1975 cells) (Fig 2).

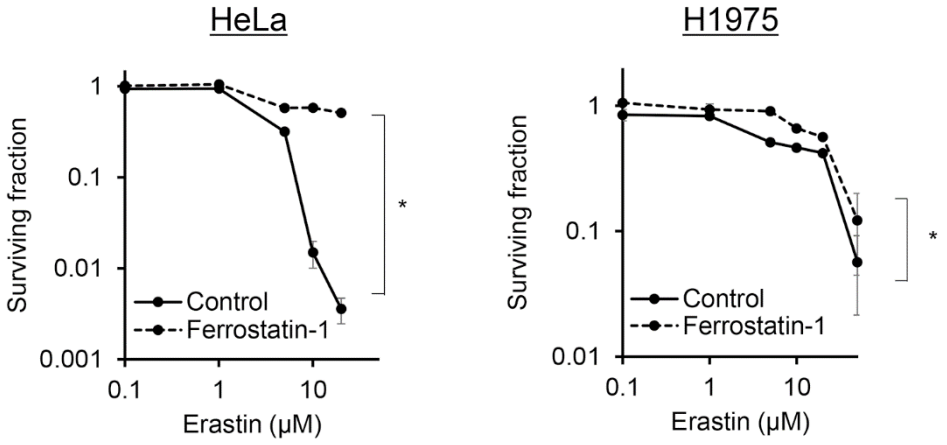

Fig 2. Ferrostatin-1 suppressed erastin cytotoxicity in human adenocarcinoma cell lines.

Clonogenic assay of the HeLa and NCI-H1975 cells. The cells were treated with erastin alone or in combination with 1.0 μM ferrostatin-1 for 24 h. All data are expressed as mean ± S.E. (n = 3, *p < 0.0001, two-way ANOVA)

Erastin treatment decreases intracellular concentrations of antioxidants.

Figs. 3A, and B show the expression level of the GPX4 protein in the HeLa and NCI-H1975 cells incubated with erastin for 24 h. The expression levels of GPX4 in both the cancer cell lines treated with erastin were significantly lower than those in nontreated cells. The intracellular GSH concentrations in the nontreated HeLa and NCI-H1975 cells

were 181.9 ± 3.9 and 133.6 ± 8.0 nmol/mg protein, respectively (Fig 3C). Treatment with erastin significantly reduced the total glutathione and GSH concentrations in a dose-dependent manner (Tukey-Kramer test, HeLa Control vs 2 μM Erastin $p < 0.01$, HeLa Control vs 10 μM Erastin $p < 0.01$, HeLa 2 μM Erastin vs 10 μM Erastin $p < 0.01$, NCI-H1975 Control vs 2 μM Erastin $p < 0.01$, NCI-H1975 Control vs 10 μM Erastin $p < 0.01$, NCI-H1975 2 μM Erastin vs 10 μM Erastin $p < 0.05$) in both the cell lines; total glutathione concentrations of the HeLa and NCI-H1975 cells treated with 10 μM decreased to 3.0% and 3.5%, respectively, and their GSH concentrations decreased to 1.0% and 3.2%, respectively (Fig 3C).

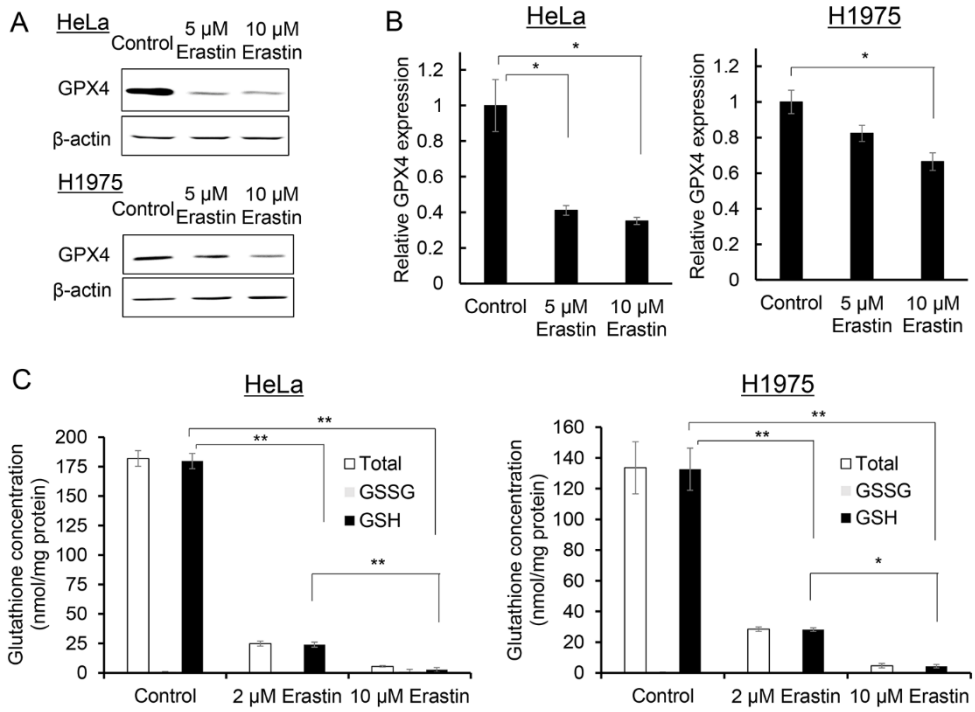

Fig 3. Erastin decreased GPX4 protein expression levels and intracellular

glutathione concentrations in human adenocarcinoma cell lines.

Western blotting of GPX4 expressions was performed on the HeLa and NCI-H1975 cells 24 h after the erastin treatment (A), and the images were analyzed to calculate the relative GPX4 expression levels in the HeLa and NCI-H11975 cells (B). The intracellular glutathione concentrations, including the total glutathione, GSH, and GSSG in the HeLa and NCI-H1975 cells, were quantified 24 h after the erastin treatment (C). All data are expressed as mean ± S.E. (n = 3, *$p < 0.05$, **$p < 0.01$, Tukey-Kramer test)

Erastin enhances X-ray-induced cell death.

The radiosensitizing effects of erastin on the HeLa and NCI-H1975 cells were evaluated (Fig 4). The treatment with a combination of erastin and X-ray irradiation significantly decreased the survival of both the cancer cell lines (two-way ANOVA, $p < 0.0001$ for treatment with erastin and $p < 0.0001$ for X-ray irradiation in both the HeLa and NCI-H1975 cells) (Fig 4). The 10% lethal doses (D_{10}) for the X-irradiated HeLa cells with and without erastin treatment were 10.24 and 8.10 Gy, respectively (sensitizer enhancement ratio [SER] = 1.27). Similarly, the D_{10} values for the X-irradiated NCI-H1975 cells with and without erastin treatment were 6.11 and 4.42 Gy, respectively (SER = 1.38).

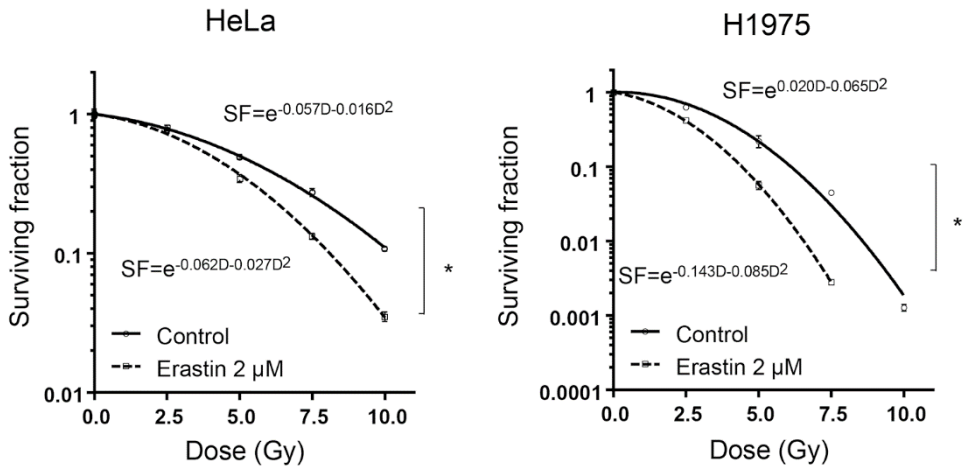

Fig 4. Erastin sensitized human adenocarcinoma cell lines to X-ray irradiation.

The radiosensitizing effect of treatment with erastin was evaluated with a clonogenic survival assay of the HeLa and NCI-H1975 cells. Before X-ray irradiation, the cells were treated with 2 μM erastin for 24 h. The survival curves of both the cell lines were fit into a linear quadratic (LQ) model using GraphPad Prism 7. All data are expressed as mean ± S.E. (n = 3, *$p < 0.0001$, two-way ANOVA) SF = Surviving fraction, D = Dose.

Treatment with erastin potentiates radiotherapy efficacy and decreases glutathione concentration in tumor xenograft models.

Effective treatment course for in vivo erastin administration was determined before the combination treatment of erastin and X-irradiation. Glutathione quantification assay revealed that the intratumoral GSH concentration was decreased in the tumor-bearing mice treated with erastin (15 mg/kg/day) for 3 days (Fig 5). The tumor-bearing

mice treated with both erastin administration and radiotherapy showed significant tumor growth suppression, while the mice treated with erastin administration or radiotherapy alone showed no tumor growth suppression (Fig 6A). The values of tumor volume (mean ± S.E) at 14 days after irradiation were 1753.84 ± 288.67 mm^3 for Control, 1738.52 ± 309.95 mm^3 for X-ray alone, 1719.07 ± 203.13 mm^3 for erastin alone, and 1079.89 ± 227.84 mm^3 for erastin + X-ray. Furthermore, a glutathione quantification assay revealed that the intratumoral glutathione concentrations in erastin-treated tumors were significantly lower than those in nontreated tumors (Fig 6B).

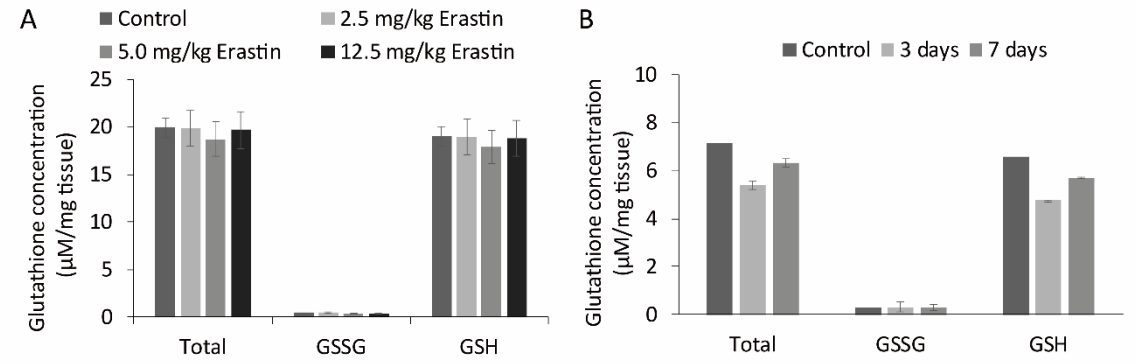

Fig 5. Three days treatment of erastin reduced intratumoral GSH concentration.

The tumor glutathione concentration in NCI-H1975 cell-transplanted mice after erastin treatment was quantified. Mice were treated with indicated dose of erastin for 24 h. The data is presented as mean ± S.E [n =5 (Control, 5.0 mg/kg, 12.5 mg/kg), n = 4 (5.0 mg/kg)] (A). Mice were treated with erastin (15 mg/kg) for 3 and 7 days at 24 h intervals. The

data is presented as mean ± S.E [n = 2 (Control), n = 3 (3 days, 7 days)] (B).

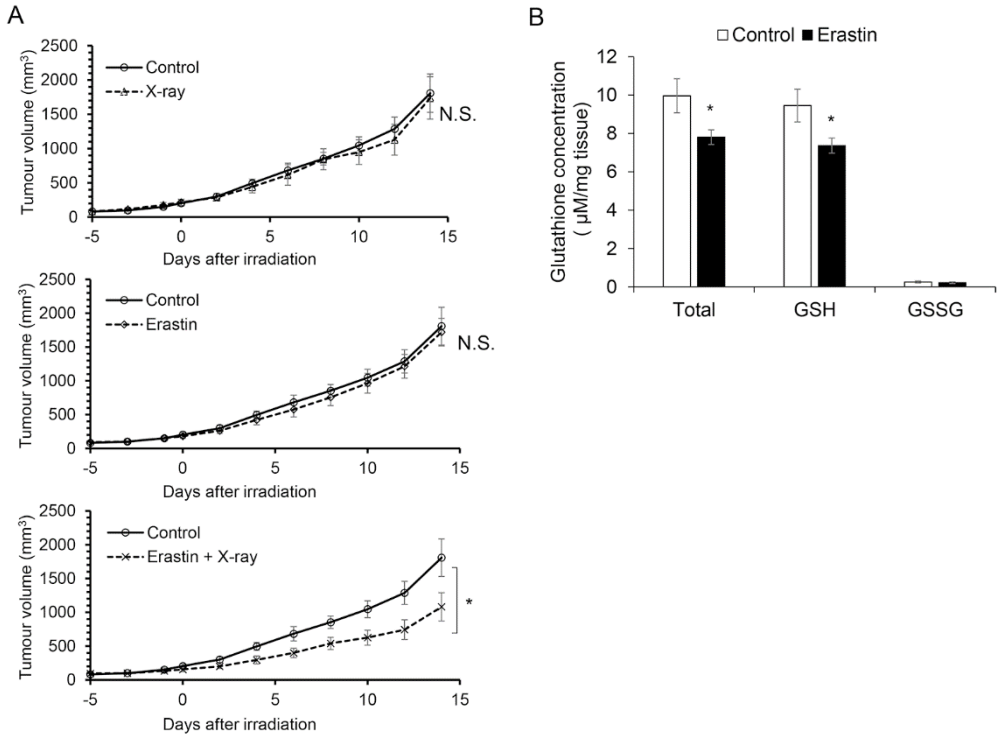

Fig 6. Treatment of NCI-H1975 cell-transplanted mice with erastin showed a tendency of sensitization to X-ray irradiation with a decrease in glutathione concentration.

NCI-H1975 cell-transplanted mice were treated with erastin (15 mg/kg intraperitoneally) for 3 days at 24 h intervals and irradiated with X-rays at a dose of 3 Gy. The data are expressed as mean ± S.E. A statistical analysis was performed with repeated-measures two-way ANOVA [n = 5 (Control, X-ray, Erastin), n = 6 (Erastin + X-ray), *$p < 0.05$] (A). The glutathione concentration was quantified in erastin-treated or nontreated NCI-H1975 cell-transplanted mice. Mice were treated with erastin as described above. The

data are expressed as mean ± S.E (n = 7, *$p < 0.05$, Student's t-test) (B).

Erastin treatment does not make differences to the cellular iron homeostasis between HeLa and NCI-H1975 cells.

Intracellular iron concentration of HeLa and NCI-H1975 cells were measured by ICP-AES. Twenty-four h erastin treatment did not alter the intracellular iron concentration of the both cell lines (Fig 7A). Moreover, western blot assay revealed that erastin treatment did not affect the TfR1 protein expression levels of HeLa and NCI-H1975 cells (Fig 7B, C).

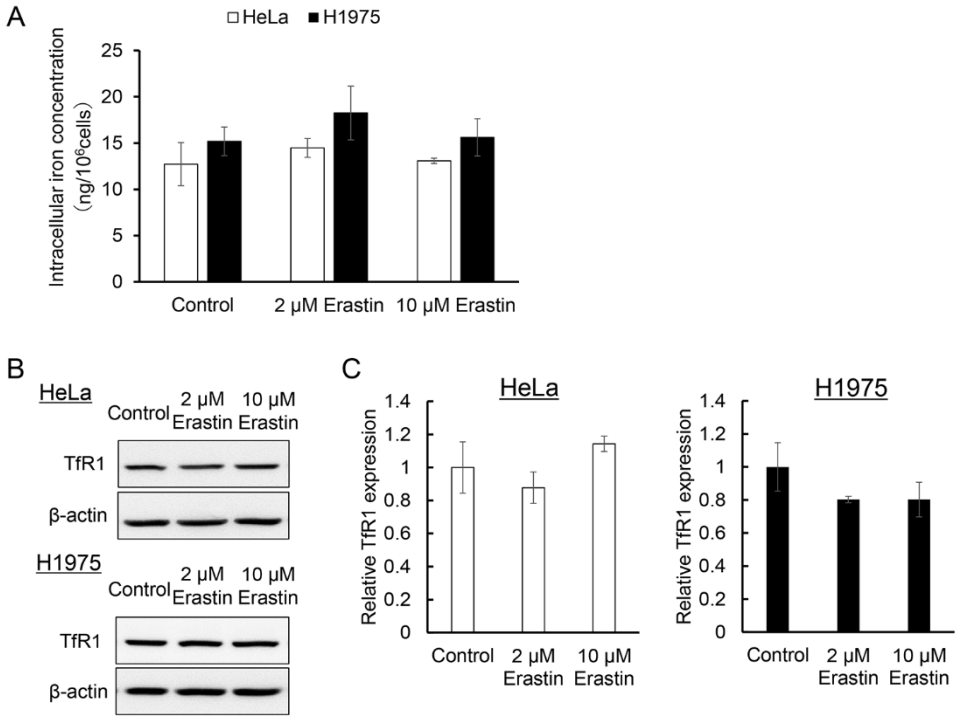

Fig 7. Erastin treatment did not affect intracellular iron concentration and TfR1

protein expression level in both HeLa and NCI-H1975 cells.

Intracellular iron concentrations of HeLa and NCI-H1975 cells were measured by ICP-AES. Both cells were treated with erastin for 24 h (A). Western blot analysis of TfR1 protein expressions was performed on HeLa and NCI-H1975 cells after 24 h erastin treatment (B), and the images were analyzed to calculate the relative TfR1 protein expression levels in both cells (C). All the data are presented as mean ± S.E. (n = 3)

Discussion

In this study, I provided new findings on the ferroptosis inducer erastin in association with cancer sensitivity to X-ray irradiation. Erastin showed dose-dependent toxicity, and ferroptosis inhibitor ferrostatin-1 partly suppressed this effect in both the human adenocarcinoma cell lines, although the inhibitory rate in the NCI-H1975 cells was smaller than that in the HeLa cells (Fig 2). In both the cell lines, the expression level of GPX4, which is a member of the glutathione peroxidase family and plays a key role in protecting cells from oxidative damage by preventing membrane lipid peroxidation, decreased after treatment with erastin, but the NCI-H1975 cells showed a smaller decrease in the GPX4 expression level compared to the HeLa cells (Figs 3A, B). However, erastin even at low concentrations markedly decreased the glutathione concentration in

both the cell lines (Fig 3C). The clonogenic survival assay revealed that the radiosensitivities of the HeLa and NCI-H1975 cells were increased when X-ray irradiation was performed after the treatment with 2 μM erastin (Fig 4). Furthermore, in vivo investigations using NCI-H1975 cell-transplanted mouse models indicated the significant radiosensitizing effect of erastin accompanied by a decrease in the tumor glutathione concentration (Fig 6).

Erastin was discovered as a direct xCT inhibitor (Dixon et al., 2012; Yagoda et al., 2007; Sato et al., 2018). Since glutathione synthesis is regulated by the cellular uptake of cystine, inhibition of xCT leads to the suppression of GSH synthesis (Sato et al., 2018; Bridges et al., 2001). Erastin is also implicated in iron absorption and accumulation, which results in the synthesis of ROS and lipid peroxidase (Gao et al., 2015; Gao et al., 2016). Thus, the iron-dependent cell death is considered to be induced by reduction in antioxidants and accumulation of free radicals. The association between antioxidants, such as glutathione or glutathione peroxidase, and tumor therapy resistance has been studied for a decade (Yant et al., 2003; Huang et al., 2003; Sleire et al., 2015; Rodman et al., 2016). These studies showed that glutathione depletion decreases the radio- and chemotherapy resistance of breast cancers and glioma cells, indicating the potential of erastin as a radiosensitizer. GPX4 is a key regulator for ferroptosis. Its major function is

to reduce lipid-peroxides using GSH as a substrate. In addition, GPX4 plays a role in the repair of DNA damage by reducing thymidine peroxides (Bao et al., 1997).

The present study revealed that the radiosensitizing effect of erastin in the two human adenocarcinoma cell lines and its dependency on the depletion of GSH levels by erastin, although, there were several differences between these cell lines. In the erastin cytotoxicity assay, the inhibitory effect of ferrostatin-1 was lesser on the NCI-H1975 cells than on HeLa cells. This finding indicates that treatment with erastin did not induce ferroptosis strongly in NCI-H1975 cells compared to HeLa cells. The difference in the suppression levels of GPX4 protein expression between NCI-H1975 and HeLa cells after treatment with erastin also supports this finding. Nevertheless, in vitro and in vivo experiments showed the radiosensitizing effect of erastin on both the adenocarcinoma cell lines. Contrary to the GPX4 protein expression, the intracellular and tumor glutathione concentrations in both the adenocarcinoma cell lines markedly decreased after the treatment with erastin. Thus, decrease in glutathione concentrations is the key factor sensitizing cancer cells to X-ray irradiation. Further, SER of erastin was higher in the NCI-H1975 cells despite the high basal GSH concentration in the HeLa cells. These differences were probably caused by the influence on iron metabolism. Iron transport is mainly mediated by the transferrin–transferrin receptor (TfR) complex in most cells.

Several cancer cell lines express higher levels of the TfR1 protein compared to the normal cells, and the TfR1 expression level is correlated with the malignancy (Högemann-Savellano et al., 2003; Habashy et al., 2010; White et al., 1990). Hence, intracellular iron and TfR1 have been considered as the targets of cancer therapies (Shen et al., 2018). However, the intracellular iron measurement by ICP-AES and western blot analysis for TfR1 protein of the HeLa and NCI-H1975 cells revealed that treatment with erastin did not show any significant influence on the iron metabolism of either cell line (Fig 7). Reduction in the intracellular GSH concentration causes radiosensitizing effect on several cancer cell lines (Sleire et al., 2015; Rodman et al., 2016; Vos et al., 1984; Yi et al., 1994). However, some studies showed no correlation between basal GSH concentration and radiosensitivity of cancer cell lines (Carney et al., 1983; Morstyn et al., 1984; Bristow et al., 1990). Thus, the difference in radiosensitivities of the HeLa and NCI-H1975 cells revealed in the present study may be caused by not only the GSH concentration but also other genetic backgrounds. The mutation status of epidermal growth factor receptor is considered to affect the radiosensitivity of non-small cell lung carcinoma, including the NCI-H1975 cells (Sartor, 2003; Yagishita et al., 2015; Amornwichet et al., 2015).

Compared to an in vitro GSSG/GSH quantification study (Fig 3C), an in vivo study has shown a relatively weak effect on GSH reduction (Fig 6B). The reason for this

can be explained by the pharmacokinetics of erastin because erastin has low water solubility, and recent studies showed a poor metabolic stability in a mouse liver microsome assay (Yang et al., 2014). Consequently, I conducted a preliminary in vivo study to determine the suitable timing for treatment with erastin. Based on it, I selected a 3-day erastin administration protocol, which was the most effective treatment course (Fig 5).

Compounds other than erastin can induce ferroptosis. xCT inhibitors, such as sulfasalazine, glutamine, and sorafenib, can induce both ferroptosis and glutathione depletion (Stockwell et al., 2017). Thus, in addition to erastin, these ferroptosis inducers may have a radiosensitizing effect on cancer cells. However, all ferroptosis inducers cannot sensitize cancer cells to X-ray irradiation. Different types of ferroptosis inducers such as RSL3 and DPI compounds, were identified as inhibitors of GPX4 (yang et al., 2014). Since these compounds can induce ferroptosis without glutathione depletion, they may not have a radiosensitizing effect. However, there have been only a few studies on the correlation between X-ray irradiation and these compounds, and further investigations are required to verify this hypothesis.

In my previous investigation using another xCT inhibitor, sulfasalazine, I demonstrated that the pretreatment with sulfasalazine decreased intratumoral glutathione

concentration, induced a high frequency of cellular DNA damage indicated by γ-H2AX staining, and an enhanced susceptibility to radiotherapy in mouse melanoma (Nagane et al., 2018). Sulfasalazine is also a ferroptosis inducer (Dixon et al., 2012), and the results obtained in this study using erastin correspond to those of our previous study. A more recent study has shown that xCT inhibition induced by erastin sensitized the breast cancer cell lines to gamma radiation (Cobler et al., 2018). In addition, the results of the present study showed a radiosensitizing effect on the cervical and lung adenocarcinoma cell lines, indicating that the combination of treatment with erastin and radiotherapy is applicable to a wide range of cancer types. Moreover, my investigation was designed for X-ray irradiation with a linear accelerator. In clinical use, linear accelerators have the advantage over cobalt-60 machines owing to their wide range of applications in cancer therapy and ease of use (Healy et al., 2017). Therefore, my data on the radiosensitizing ratio can be easily extended to clinical studies. Moreover, recent studies showing that erastin sensitizes cancer cells to gamma radiation have strengthened my findings.

In conclusion, the present study indicates the novel potential of ferroptosis-inducing agents as radiosensitizing drugs. Furthermore, considering previous studies showing successful treatment with ferroptosis-induced cancer therapies in combination with chemotherapies, further advancements of ferroptosis-induced cancer therapies are

expected.

Chapter 2

Development of a nuclear imaging probe to predict therapeutic effect of ferroptosis-targeting cancer therapy

Introduction

In chapter 1, I investigated a novel cancer therapeutic strategy targeting ferroptosis combined with X-irradiation, which may broaden the potentials of ferroptosis-targeting cancer therapy. As mentioned above, several ferroptosis inducers have already been known to show the antitumor effects, however, it can be presumed that the efficacy of the ferroptosis-targeting cancer therapy may be different among the cancer types. The drug screening test in a past study reported that the sensitivity to ferroptosis inducer vary among the types of cancer cells (Yang et al., 2014). Indeed, my study in chapter 1 also demonstrated that the sensitivity to erastin was different between HeLa and NCI-H1975 cell lines. To adapt this ferroptosis-targeting therapy to individual patients effectively, development of a technique for predicting sensitivity of cancer to the therapy is required. However, to my knowledge, no study has been reported to establish promising tools for predicting the sensitivity. Because, a trigger for ferroptosis, lipidperoxides are produced by an intracellular iron, a major iron uptake pathway via transferrin-TfR complex can be expected as a key factor for cancer sensitivity of ferroptosis. Past study indicates that the

serum iron transporter transferrin plays a crucial role in ferroptosis induction and also, the expression levels of TfR1 protein in cancer cells correlate with the sensitivity of ferroptosis (Gao et al., 2015; Yang et al., 2008). Therefore, I hypothesized that the cellular uptake amount of transferrin correlates to the cancer sensitivity of ferroptosis. In chapter 2, with the aim of developing a prediction method of cancer sensitivity to ferroptosis-inducing drug, I developed a transferrin-based nuclear imaging probe that allows non-invasive quantification of transferrin uptake levels in cancers.

Materials & Methods

Reagents

Erastin was purchased from AdooQ Bioscience, human-apo-transferrin (aTf) and human-holo-transferrin (hTf, iron bound form) was purchased from Sigma-Aldrich, and the following antibodies were used for western blotting: anti-TfR1 (Cat. No. ab84026, Abcam), anti-β-actin (Sigma-Aldrich), and horseradish peroxidase-conjugated secondary antibodies (Promega, Madison, WI).

Conjugation of p-isothiocyanatobenzyl-1,4,7-triazacyclononane-1,4,7-triacetic acid (NOTA) to aTf

NOTA-aTf was synthesized by mixing aTf in 0.1 M carbonate buffer (1.0 mg/ml, pH 9.0) with a 16-fold molar excess of p-isothiocyanatobenzyl-NOTA (Macrocyclics, Inc.) in DMSO for one hour at 37°C. The DMSO concentration was below 5% in this reaction mixture. NOTA-aTf was purified and the solvent was replaced by PBS (-) with a PD-10 column (GE Healthcare Life Sciences, Buckinghamshire, UK) and an Amicon Ultra 50K device (Merk Millipore).

Radiolabeling and conversion to hTf

$^{68}GaCl_3$ was eluted from $^{68}Ge/^{68}Ga$-generator (Galli Eo®, IRE ELiT, Fleurus, Bergium). The $^{68}GaCl_3$ solution was evaporated and resolved in 10 µL of 0.1 M HCl. The solvent (phosphate buffer) of NOTA-aTf was replaced with 0.1 M 2-[4-(2-hydroxyethyl)-1-piperazinyl] ethanesulfonic acid (HEPES) (pH 5.5) by using an Amicon Ultra 50K device. To the NOTA-aTf solution, the $^{68}GaCl_3$ solution (c.a. 10 µL) was added and adjusted to 1.0 mg/mL with 0.1 M HEPES buffer. The mixture was incubated at 25°C for 5 minutes to give NOTA-aTf labeled with ^{68}Ga (^{68}Ga-NOTA-aTf). After the incubation, the solvent was replaced with 0.01 M $NaHCO_3$ (pH 7.4) by using the Amicon-Ultra 50K device. To obtain NOTA-hTf labeled with ^{68}Ga (^{68}Ga-NOTA-aTf), ^{68}Ga-NOTA-aTf was reacted with same volume of 2 mM $FeCl_3$, 40 mM citric acid solution (pH 7.4) at 37°C

for 30 minutes (Fig 8). Synthesized ^{68}Ga-NOTA-aTf and ^{68}Ga-NOTA-hTf was purified with a PD-10 column and the solvent was replaced by PBS (-) with an Amicon Ultra 50K device. The resultant solution was used for in vitro uptake study.

The radiochemical purities of ^{68}Ga-NOTA-aTf and ^{68}Ga-NOTA-hTf were confirmed by radio-thin layer chromatography (TLC) and high-performance liquid chromatography (HPLC) analysis. TLC analysis was performed with reversed-phase TLC plates (RP-18 F254 S, Merck Millipore) and 0.02 M citric acid- 0.05 M ethylenediaminetetraacetic acid (EDTA) (pH 5.0) as the mobile phase. The TLC chromatograms were obtained by autoradiography (FLA-7000IR; GE Healthcare Life Science). Size exclusion HPLC was performed with a TSKgel SuperSW2000 column (Tosoh Bioscience LLC, King of Prussia, PV) connected with a TSK SuperSW guard column (Tosoh Bioscience LLC). Phosphate buffer (0.3 M NaCl, 0.01 M phosphate buffer [pH 7.0]) was used as the mobile phase (flow rate, 0.4 mL/min; wave length, 280 nm). The chromatograms were obtained using a HPLC system equipped with a multi-wavelength UV detector (SPD-20A UV/VIS detector, Shimadzu) and a radioactivity detector (Raytest Gabi Star, Straubenhardt, Germany).

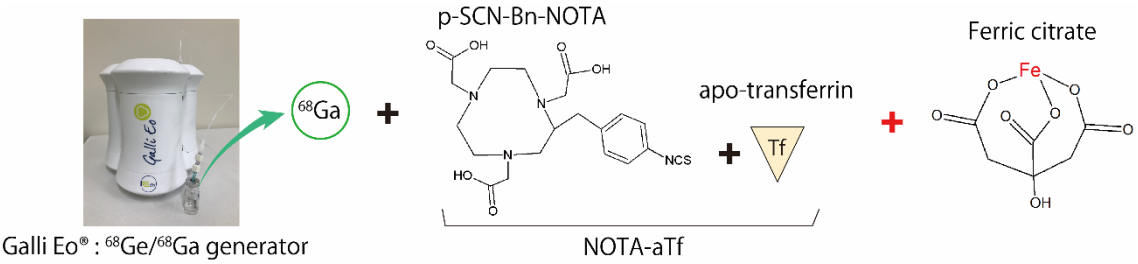

Fig 8. Reaction scheme of ^{68}Ga-NOTA-hTf

Number of chelators conjugated with aTf

Matrix-assisted laser desorption-ionization time-of-flight mass spectrometry (MALDI-TOF-MS) was performed using ultrafleXtreme (Bruker Daltonics, Bremen, Germany) to examine the number of chelators conjugated with aTf. Non-conjugated- and chelator-conjugated aTf were desalted with PD Spin Trap G-25 (GE Healthcare Life Science). 3,5-Dimethoxy-4-hydroxycinnamic acid (Tokyo Chemical Industry Co., Tokyo, Japan) at 10 mg/mL in 1:1 acetonitrile/H_2O with 0.1% trifluoroacetic acid was used as the MALDI matrix. For each sample, the measurements were repeated four times. The measured mass difference between aTf and NOTA-aTf was divided by the mass value of single NOTA, and the resulting values represented the average number of NOTA that were conjugated to aTf.

Iron concentration

The concentration of transferrin-bound iron was determined by ICP-AES (ICPE-9000, Shimadzu). Before the ICP-AES measurement, each sample (0.5 mg) were pre-digested in 10 mL of 4% ultra-high purity nitric acid (KANTO CHEMICAL Co., Inc.) and micro-wave heated at 200°C for 20 min with a microwave digestion system (ETHOS-One, Milestone, Sorisole, Italy). In order to calculate iron concentration, iron standard solution (AccuStandard Inc.) was prepared at 5, 10, 50, 100, 500 ppm.

Cell culture

Human renal cancer cell lines, A498 and 786-O cells, were purchased from American Type Culture Collection. These cells were grown in the RPMI-1640 medium supplemented with 10% fetal bovine serum and 100 units/mL of penicillin-streptomycin. The cells were maintained at 37°C in 5% CO_2.

Clonogenic survival assay

The sensitivity of the cancers to a ferroptosis inducer erastin in vitro was evaluated by a clonogenic assay. An appropriate number of tumor cells attached to 60 mm dishes were treated with erastin. After the drug treatment for 24 hours, the compounds were removed by replacing the medium with a fresh one and then the cells

were incubated in a humidified 5% CO_2 atmosphere at 37°C for nine days. The cell colonies were fixed with methanol, stained with the Giemsa solution, and counted under a microscope. Only the colonies containing more than 50 cells were counted as surviving colonies.

SDS-PAGE and western blotting

Expression levels of TfR1 in the cancer cells were evaluated by western blot analysis. The A498 and 786-O cells were collected and lysed in a RIPA buffer with a protease inhibitor cocktail and subjected to two freeze–thaw cycles. The lysed cells were centrifuged at 15,000×g for 20 min at 4°C, and the supernatants were collected as protein samples. Laemmli's sample buffer was added to the supernatants, and the mixture was boiled for 5 min. Proteins were separated by SDS-PAGE and transferred onto a PVDF membrane at 60 V in a transfer buffer (25 mM Tris, 192 mM glycine, and 20% methanol) for 60 min at 4°C. The membrane was probed overnight with specific antibodies diluted with TBST (10 mM Tris-HCl [pH 7.4], 0.1 M NaCl and 0.1% Tween-20) containing 5% skim milk at 4°C. After probing with HRP-conjugated secondary antibodies, the bound antibodies were detected with an Immobilon® western HRP substrate. Densitometry was performed using Multi Gauge V3.0 software.

Cell uptake assay

A498 and 786-O cells were plated in 30 mm dishes (2.0×10^5 cells/dish). After 16 h incubation at 37°C in 5% CO_2, an aliquot (0.1 mL) of ^{68}Ga-NOTA-Tf (20 μg/mL [2.2-3.1 MBq/mL]) was added to cells maintained in 0.9 mL of RPMI-1640 containing 10% FBS and incubated for an hour. The media was removed, cells were washed twice (2×1.0 mL) with PBS. Cells were incubated (1.0 mL) with an acidic solution (0.1 M glycine, 20 mM acetic acid, pH 4.0) for 1 min to strip surface bound transferrin. Finally, cells were lysed in 1.0 mL of 0.1 M NaOH (aq.) to collect internalized activity. Radioactivity in the media, wash solution, cell surface, and intracellular fractions was measured using γ-counter (Wizard 2 2480, Perkin-Elmer, Waltham, MA). All collected data were normalized by cellular protein levels of each sample quantified with BSA protein assay.

Statistical analysis

All results are expressed as the mean ± S.E. The statistical analysis was performed using GraphPad Prism 7. Differences in TfR1 protein expression level between the two cell lines were evaluated with Student's t-test (Fig 9). The statistical significance

of erastin cytotoxicity on the two cell lines were examined with two-way ANOVA (Fig 10). Multiple comparisons for the results of cellular uptake analysis were performed with Tukey–Kramer test (Fig 11). A p-value < 0.05 was considered significant.

Results

Synthesis of ^{68}Ga-NOTA-aTf and ^{68}Ga-NOTA-hTf

The number of NOTA bound to aTf was measured by MALDI-TOF-MS. The NOTA-aTf binding ratio was 2.66 ± 0.22 NOTA/aTf (n = 3). The amount of iron bound with transferrin was measured by ICP-AES. The amount of iron in aTf and hTf, which were purchased commercially, were 90.5 and 1048.0 μg/g, respectively. In addition, the amount of iron in aTf reacted with ferric citrate was approximately 1133.3 μg/g. The radiochemical purities of ^{68}Ga-NOTA-aTf and ^{68}Ga-NOTA-hTf analyzed by TLC and HPLC were more than 96% and 92%, respectively. The radiochemical yields of ^{68}Ga-NOTA-aTf and ^{68}Ga-NOTA-hTf determined by dose calibrator were around 70% (Table 1).

Table 1. Radiochemical purity and yield of ^{68}Ga-NOTA-aTf and ^{68}Ga-NOTA-hTf.

^{68}Ga-NOTA-Tf	Apo form	Holo form
Radiochemical purity (TLC)	>98%	>98%
Radiochemical purity (HPLC)	>96%	>92%
Radiochemical yeild	72.8%	63.5%

Radiochemical purities of ^{68}Ga-NOTA-aTf and ^{68}Ga-NOTA-hTf were confirmed by TLC and HPLC analysis and the radiochemical yields were determined by dose calibrator.

TfR1 protein expression level correlates with the sensitivity to erastin in human renal cancer cell lines.

First, the TfR1 protein expression levels in human renal cancer cell lines (A498 and 786-O cells) were analyzed by western blotting and revealed that the TfR1 expression level of 786-O cells was relatively higher than A498 cells (Fig 9). In addition, clonogenic survival assay revealed that the sensitivity of 786-O cells to erastin was significantly higher than that of A498 cells (Surviving fractions of A498 and 786-O cells treated with 10 μM erastin for 24 h were 19.0% and 2.9%, respectively.) (Fig 10).

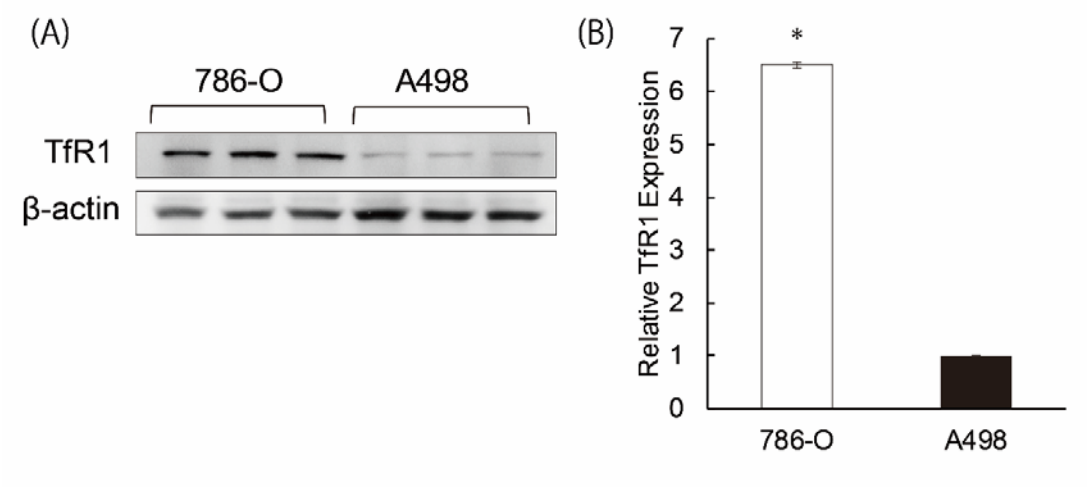

Fig 9. TfR1 protein expression levels in two human renal cancer cell lines.

Western blotting of TfR1 and β-actin expressions were performed on the A498 and 786-O cells (A), and the images were analyzed to calculate the relative TfR1 expression levels in these cell lines (B). All data are expressed as mean ± S.E. (n = 3, *$p < 0.05$, Student's t-test)

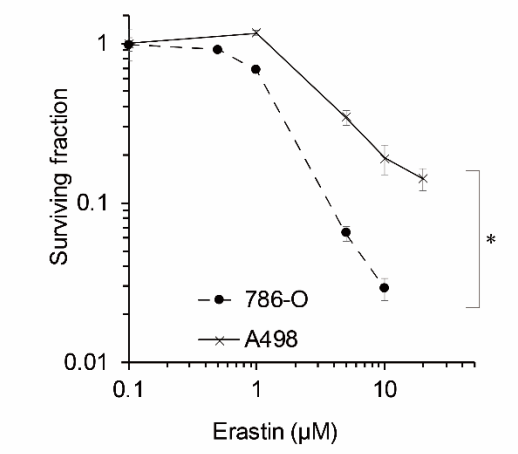

Fig 10. Clonogenic assay of erastin's cytotoxicity in human renal cancer cell lines (A498 and 786-O cells).

Cancer cells were treated with erastin (0 – 20 μM) for 24 h. All data are expressed as

mean ± S.E. (n = 3, *p < 0.05, two-way ANOVA)

^{68}Ga-NOTA-hTf highly accumulates to the 786-O cells highly expressing TfR1 protein.

Cellular uptake levels of ^{68}Ga-NOTA-aTf and ^{68}Ga-NOTA-hTf were evaluated (Fig 11). As a result, ^{68}Ga-NOTA-hTf was highly internalized than ^{68}Ga-NOTA-aTf in both cell lines. Moreover, the level of internalized ^{68}Ga-NOTA-hTf was significantly higher in 786-O cells compared to A498 cells.

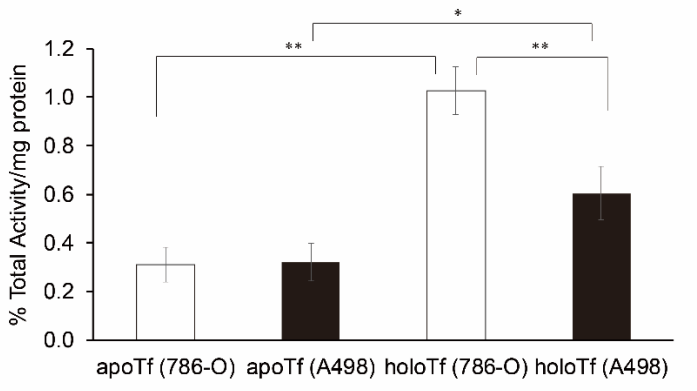

Fig 11. Cellular uptake of ^{68}Ga-NOTA-aTf and ^{68}Ga-NOTA-hTf in human renal cancer cell lines (A498 and 786-O cells).

Cancer cells were treated with ^{68}Ga-NOTA-aTf and ^{68}Ga-NOTA-hTf, and incubated at 37°C for 60 minutes. All data are expressed as mean ± S.E. (n = 3, *p < 0.05, **p < 0.01, Tukey–Kramer test)

Discussion

In this study, I obtained a basic data to establish a prediction method of ferroptosis-targeting anticancer effect. I designed a radioactive probe targeting TfR1, ^{68}Ga-labeled human transferrin conjugated with NOTA as a metal chelator. There are two forms of transferrin called as apo and holo transferrin (aTf and hTf). aTf turns into hTf, when it bounds with iron. It is known that iron-bound hTf has higher binding affinity to the receptor (Young et al., 1984). Moreover, hTf releases iron in acidic circumstance and unbound with the receptors (Klausner et al., 1983; Bali et al., 1991). On the other hand, $^{68}GaCl_3$ is known to form colloids under neutral conditions and may affect radiolabeling. Therefore, aTf was conjugated with metal chelator NOTA firstly and then radiolabeled with ^{68}Ga to synthesize ^{68}Ga-NOTA-aTf. After radiolabeling, ^{68}Ga-NOTA-aTf was reacted with excess amount of ferric citrate to form ^{68}Ga-NOTA-hTf. The amount of iron bound with transferrin was quantified using ICP-AES and revealed that aTf was fully saturated with iron by an addition of ferric citrate. With TLC, it has confirmed that addition of ferric citrate did not influence the radiochemical purity of ^{68}Ga-NOTA-hTf (Table 1). Purified ^{68}Ga-NOTA-hTf was analyzed by HPLC, which indicated successful radiosynthesis of ^{68}Ga-NOTA-hTf with a high purity (Table 1).

Two human renal cancer cell lines which I used in this study showed significant

difference in TfR1 protein expression levels (Fig 9). Erastin sensitivity in 786-O cells, which highly expresses TfR1 protein, was relatively higher than A498 cells (Fig 10). These results indicate that the TfR1 expression level in human renal cancer cell lines correlates to the sensitivity of a ferroptosis-inducer erastin. Notably, internalized amount of ^{68}Ga-NOTA-hTf was significantly higher in erastin sensitive renal cancer 786-O cells, as I expected (Fig 11). Moreover, ^{68}Ga-NOTA-aTf showed limited internalization in both cell lines, indicating that iron saturation is necessary for radiolabeled NOTA-Tf uptake by cancer cells. These results suggested that ^{68}Ga-NOTA-hTf could predict the cancer sensitivity to the ferroptosis-inducer erastin.

The previous studiesdemonstrated that the cancer sensitivity to ferroptosis inducer erastin varies among the cancer cell types (Yang et al., 2014), and suppression of TfR1 by si-RNA treatment decreases the cancer sensitivity to erastin (Yang et al., 2008). Moreover, the serum iron transporter transferrin was found to be essential for ferroptosis induction through amino acid starvation (Gao et al., 2015). As noted above, there is increasing interest in the relationship between ferroptosis and iron metabolic pathways. However, diagnostic techniques for predicting cancer ferroptosis have not been actually developed. In chapter 2, I demonstrated that sensitivity of the cancer cells to a ferroptosis inducer erastin correlates with the transferrin uptake level in renal cancer cell lines. Thus,

my study indicates for the first time to my knowledge that the radioactive probe targeting TfR1 could predict sensitivity of cancers to the treatments that induce ferroptosis. Several ferroptosis inducers have shown to attenuate chemotherapy and radiotherapy resistance and enhances their therapeutic effects (Roh et al., 2016; Yu et al., 2015; Chen et al., 2015). Therefore, ferroptosis-targeting cancer therapy is now expected to be an effective therapeutic strategy to refractory cancers. In this study, ^{68}Ga nuclide was used for radiolabeling transferrin, as ^{68}Ga can be easily obtained from a ^{68}Ge/^{68}Ga-generator. Although this positron emission nuclide has recently attracted a lot of attention as a useful radionuclide for positron emission tomography (PET), its short half-life may hamper the diagnostic imaging of labeled compounds with large molecular weight including transferrin due to the slow pharmacokinetics of the labeled compound. NOTA-hTf synthesized in this study, however, can be easily labeled with other radionuclides with longer half-lives, including ^{67}Ga, which enables us non-invasive evaluation of functional molecules. Further experiments to investigate whether the accumulated amount of radiolabeled NOTA-hTf in tumor reflects the in vivo anticancer effect of the ferroptosis inducer, are also useful for establishing diagnostic method of ferroptosis induction in cancer with nuclear medicine imaging. Thus, by diagnosing the therapeutic effect of ferroptosis-targeting cancer treatment using radiolabeled NOTA-hTf in advance, it will

become possible to provide the best cancer treatment for individual patient.

I performed investigations only in human renal cancer cell lines in the present study. Thus, it is unclear whether similar results can be obtained with cancer cells derived from other organs than kidney. Recently, several reports have shown that the sensitivities of HRAS-mutant cancers and lukemia cell line to ferroptosis induction have been correlated with TfR1 and cellular labile iron pool (Yang and Stockwell, 2008; Yang et al., 2016; Ye et al., 2019). Therefore, it can be considered that the similar results as my study are likely to be obtained even for cell types derived from the other organs. There are several key factors regulating ferroptosis other than TfR1 (e.g. xCT, GPX4, and ACSL4) (Xie et al., 2016; Stockwell et al., 2017). Thus, it is necessary to investigate the significance of those factors to ferroptosis induction.

In conclusion, my invented radiolabeled NOTA-hTf may have potential to predict therapeutic effect of ferroptosis-targeting cancer therapy in vivo. Although further studies are needed, I believe that radiolabeled NOTA-hTf could provide best approaches to individual patients.

Summary & Conclusion

Researches on a novel cell death mechanism have a potential to contribute greatly to

cancer therapy, leading to an alternative treatment strategy. In the present study, I investigated the usefulness of ferroptosis-targeting cancer therapy strategy using several types of human cancer cell lines and obtained the following results.

1. Erastin treatment enhanced therapeutic effect of X-ray irradiation treatment through glutathione depletion.
2. Erastin sensitivity correlates with TfR1 expression level of human renal cancer cell lines and ^{68}Ga-NOTA-hTf has a potential to predict erastin sensitivity of cancer cells.

From these investigations, I have demonstrated the validity of ferroptosis-targeting cancer therapy strategy. Moreover, I have successfully proposed a method for predicting therapeutic effect of the ferroptosis-targeting therapy. These studies are likely to help guide the development of novel anticancer strategy targeting ferroptosis which will make possible to provide best approaches to individual patients.

Acknowledgements

I would like to offer special thanks to my supervisor, Prof. Yuji Kuge, for his encouragement and tremendous support. This study would not have been possible without his guidance. I am deeply grateful to Dr. Hironobu Yasui. His abundantly helpful assistance and discussions were invaluable. I would like to express my sincere thanks Dr.

Kei Higashikawa for valuable advice and support. His wide knowledge and logical way of thinking will go a long way in my career as a researcher. I am deeply grateful to Dr. Naoki Miyamoto for technical support and suggestions regarding the X-ray irradiation experiments. Suggestions and discussion with Dr. Yuichi Hirata, Mr. Kenji Abo, and Mr. Sho Tomita greatly contributed to the completion of my thesis. I would like to express my gratitude to them. I thank all the members of laboratory of Integrated molecular imaging at Hokkaido University. In particular, I am deeply grateful to Ms. Reimi Kishi for technical support in the experiments. Last but not least, I thank all my family members: my father Yasuhiro, my mother Mariko, my sister Risa, as well as my grandparents. Each of them shares credit for this accomplishment; without their support, this achievement would not have been possible.

References

Amornwichet N, Oike T, Shibata A, Nirodi CS, Ogiwara H, Makino H, et al. The EGFR mutation status affects the relative biological effectiveness of carbon-ion beams in non-small cell lung carcinoma cells. Scientific Reports. 2015;5(1):11305.

Bao Y, Jemth P, Mannervik B, Williamson G. Reduction of thymine hydroperoxide by phospholipid hydroperoxide glutathione peroxidase and glutathione transferases. FEBS

Letters. 1997;410(2-3):210-2.

Bansal A, Simon MC. Glutathione metabolism in cancer progression and treatment resistance. J Cell Biol. 2018;217(7):2291-8.

Bogdan AR, Miyazawa M, Hashimoto K, Tsuji Y. Regulators of Iron Homeostasis: New Players in Metabolism, Cell Death, and Disease. Trends Biochem Sci. 2016;41(3):274-86.

Bridges CC, Kekuda R, Wang H, Prasad PD, Mehta P, Huang W, et al. Structure, function, and regulation of human cystine/glutamate transporter in retinal pigment epithelial cells. Invest Ophthalmol Vis Sci. 2001;42(1):47-54.

Bristow RG, Hardy PA, Hill RP. Comparison between in vitro radiosensitivity and in vivo radioresponse of murine tumor cell lines I: parameters of in vitro radiosensitivity and endogenous cellular glutathione levels. International Journal of Radiation Oncology*Biology*Physics. 1990;18(1):133-45.

Bystrom LM, Rivella S. Cancer cells with irons in the fire. Free Radic Biol Med. 2015;79:337-42.

Carney DN, Mitchell JB, Kinsella TJ. In vitro radiation and chemotherapy sensitivity of established cell lines of human small cell lung cancer and its large cell morphological variants. Cancer Res. 1983;43(6):2806-11.

Chen L, Li X, Liu L, Yu B, Xue Y, Liu Y. Erastin sensitizes glioblastoma cells to temozolomide by restraining xCT and cystathionine-γ-lyase function. Oncol Rep. 2015;33(3):1465-74.

Cobler L, Zhang H, Suri P, Park C, Timmerman LA. xCT inhibition sensitizes tumors to γ-radiation via glutathione reduction. Oncotarget. 2018;9(64):32280-97.

Deng Z, Manz DH, Torti SV, Torti FM. Iron-responsive element-binding protein 2 plays an essential role in regulating prostate cancer cell growth. Oncotarget. 2017;8(47):82231-43.

Dixon SJ, Lemberg KM, Lamprecht MR, Skouta R, Zaitsev EM, Gleason CE, et al. Ferroptosis: an iron-dependent form of nonapoptotic cell death. Cell. 2012;149(5):1060-72.

Dixon SJ, Patel DN, Welsch M, Skouta R, Lee ED, Hayano M, et al. Pharmacological inhibition of cystine-glutamate exchange induces endoplasmic reticulum stress and ferroptosis. Elife. 2014;3:e02523.

Elford HL, Freese M, Passamani E, Morris HP. Ribonucleotide reductase and cell proliferation. I. Variations of ribonucleotide reductase activity with tumor growth rate in a series of rat hepatomas. J Biol Chem. 1970;245(20):5228-33.

Gao M, Monian P, Quadri N, Ramasamy R, Jiang X. Glutaminolysis and Transferrin

Regulate Ferroptosis. Mol Cell. 2015;59(2):298-308.

Gao M, Monian P, Pan Q, Zhang W, Xiang J, Jiang X. Ferroptosis is an autophagic cell death process. Cell Res. 2016;26(9):1021-32.

Habashy HO, Powe DG, Staka CM, Rakha EA, Ball G, Green AR, et al. Transferrin receptor (CD71) is a marker of poor prognosis in breast cancer and can predict response to tamoxifen. Breast Cancer Res Treat. 2010;119(2):283-93.

Healy BJ, van der Merwe D, Christaki KE, Meghzifene A. Cobalt-60 Machines and Medical Linear Accelerators: Competing Technologies for External Beam Radiotherapy. Clin Oncol (R Coll Radiol). 2017;29(2):110-5.

Högemann-Savellano D, Bos E, Blondet C, Sato F, Abe T, Josephson L, et al. The transferrin receptor: a potential molecular imaging marker for human cancer. Neoplasia. 2003;5(6):495-506.

Huang X. Iron overload and its association with cancer risk in humans: evidence for iron as a carcinogenic metal. Mutat Res. 2003;533(1-2):153-71.

Lu B, Chen XB, Ying MD, He QJ, Cao J, Yang B. The Role of Ferroptosis in Cancer Development and Treatment Response. Front Pharmacol. 2017;8:992.

Luo M, Wu L, Zhang K, Wang H, Zhang T, Gutierrez L, et al. miR-137 regulates ferroptosis by targeting glutamine transporter SLC1A5 in melanoma. Cell Death Differ.

2018;25(8):1457-72.

Manz DH, Blanchette NL, Paul BT, Torti FM, Torti SV. Iron and cancer: recent insights. Ann N Y Acad Sci. 2016;1368(1):149-61.

Mooney MR, Geerts D, Kort EJ, Bachmann AS. Anti-tumor effect of sulfasalazine in neuroblastoma. Biochem Pharmacol. 2019.

Morstyn G, Russo A, Carney DN, Karawya E, Wilson SH, Mitchell JB. Heterogeneity in the radiation survival curves and biochemical properties of human lung cancer cell lines. J Natl Cancer Inst. 1984;73(4):801-7.

Muckenthaler MU, Galy B, Hentze MW. Systemic iron homeostasis and the iron-responsive element/iron-regulatory protein (IRE/IRP) regulatory network. Annu Rev Nutr. 2008;28:197-213.

Muckenthaler MU, Rivella S, Hentze MW, Galy B. A Red Carpet for Iron Metabolism. Cell. 2017;168(3):344-61.

Nagane M, Kanai E, Shibata Y, Shimizu T, Yoshioka C, Maruo T, et al. Sulfasalazine, an inhibitor of the cystine-glutamate antiporter, reduces DNA damage repair and enhances radiosensitivity in murine B16F10 melanoma. PLoS One. 2018;13(4):e0195151.

Rodman SN, Spence JM, Ronnfeldt TJ, Zhu Y, Solst SR, O'Neill RA, et al. Enhancement of Radiation Response in Breast Cancer Stem Cells by Inhibition of Thioredoxin- and

Glutathione-Dependent Metabolism. Radiat Res. 2016;186(4):385-95.

Roh JL, Kim EH, Jang HJ, Park JY, Shin D. Induction of ferroptotic cell death for overcoming cisplatin resistance of head and neck cancer. Cancer Lett. 2016;381(1):96-103.

Sartor CI. Epidermal growth factor family receptors and inhibitors: Radiation response modulators. Seminars in Radiation Oncology. 2003;13(1):22-30.

Sato M, Kusumi R, Hamashima S, Kobayashi S, Sasaki S, Komiyama Y, et al. The ferroptosis inducer erastin irreversibly inhibits system x c − and synergizes with cisplatin to increase cisplatin's cytotoxicity in cancer cells. Sci Rep. 2018;8(1):968.

Shen Y, Li X, Dong D, Zhang B, Xue Y, Shang P. Transferrin receptor 1 in cancer: a new sight for cancer therapy. Am J Cancer Res. 2018;8(6):916-31.

Shibata Y, Yasui H, Higashikawa K, Miyamoto N, Kuge Y. Erastin, a ferroptosis-inducing agent, sensitized cancer cells to X-ray irradiation via glutathione starvation *in vitro* and *in vivo*. PLoS ONE 14(12): e0225931.

Sleire L, Skeie BS, Netland IA, Førde HE, Dodoo E, Selheim F, et al. Drug repurposing: sulfasalazine sensitizes gliomas to gamma knife radiosurgery by blocking cystine uptake through system Xc-, leading to glutathione depletion. Oncogene. 2015;34(49):5951-9.

Sontheimer H, Bridges RJ. Sulfasalazine for brain cancer fits. Expert Opin Investig Drugs.

2012;21(5):575-8.

Stockwell BR, Friedmann Angeli JP, Bayir H, Bush AI, Conrad M, Dixon SJ, et al. Ferroptosis: A Regulated Cell Death Nexus Linking Metabolism, Redox Biology, and Disease. Cell. 2017;171(2):273-85.

Tagde A, Singh H, Kang MH, Reynolds CP. The glutathione synthesis inhibitor buthionine sulfoximine synergistically enhanced melphalan activity against preclinical models of multiple myeloma. Blood Cancer J. 2014;4:e229.

Torti SV, Manz DH, Paul BT, Blanchette-Farra N, Torti FM. Iron and Cancer. Annu Rev Nutr. 2018;38:97-125.

Traverso N, Ricciarelli R, Nitti M, Marengo B, Furfaro AL, Pronzato MA, et al. Role of glutathione in cancer progression and chemoresistance. Oxid Med Cell Longev. 2013;2013:972913.

Villablanca JG, Volchenboum SL, Cho H, Kang MH, Cohn SL, Anderson CP, et al. A Phase I New Approaches to Neuroblastoma Therapy Study of Buthionine Sulfoximine and Melphalan With Autologous Stem Cells for Recurrent/Refractory High-Risk Neuroblastoma. Pediatr Blood Cancer. 2016;63(8):1349-56.

Vos O, Van Der Schans GP, Roos-Verhey WSD. Effects of BSO and DEM on thiol-level and radiosensitivity in HeLa cells. 1984;10(8):1249-53.

White S, Taetle R, Seligman PA, Rutherford M, Trowbridge IS. Combinations of anti-transferrin receptor monoclonal antibodies inhibit human tumor cell growth in vitro and in vivo: evidence for synergistic antiproliferative effects. Cancer Res. 1990;50(19):6295-301.

Yagishita S, Horinouchi H, Katsui Taniyama T, Nakamichi S, Kitazono S, Mizugaki H, et al. Epidermal Growth Factor Receptor Mutation Is Associated With Longer Local Control After Definitive Chemoradiotherapy in Patients With Stage III Nonsquamous Non–Small-Cell Lung Cancer. 2015;91(1):140-8.

Yagoda N, von Rechenberg M, Zaganjor E, Bauer AJ, Yang WS, Fridman DJ, et al. RAS-RAF-MEK-dependent oxidative cell death involving voltage-dependent anion channels. Nature. 2007;447(7146):864-8.

Yang WS, Stockwell BR. Synthetic lethal screening identifies compounds activating iron-dependent, nonapoptotic cell death in oncogenic-RAS-harboring cancer cells. Chem Biol. 2008;15(3):234-45.

Yang WS, SriRamaratnam R, Welsch ME, Shimada K, Skouta R, Viswanathan VS, et al. Regulation of ferroptotic cancer cell death by GPX4. Cell. 2014;156(1-2):317-31.

Yant LJ, Ran Q, Rao L, Van Remmen H, Shibatani T, Belter JG, et al. The selenoprotein GPX4 is essential for mouse development and protects from radiation and oxidative

damage insults. Free Radic Biol Med. 2003;34(4):496-502.

Yi X, Ding L, Jin Y, Ni C, Wang W. The toxic effects, GSH depletion and radiosensitivity by BSO on retinoblastoma. International Journal of Radiation Oncology*Biology*Physics. 1994;29(2):393-6.

Yu Y, Xie Y, Cao L, Yang L, Yang M, Lotze MT, et al. The ferroptosis inducer erastin enhances sensitivity of acute myeloid leukemia cells to chemotherapeutic agents. Mol Cell Oncol. 2015;2(4):e1054549.